Journal of Power Sources 196 (2011) 788–792

Contents lists available at ScienceDirect

Journal of Power Sources

journal homepage: www.elsevier.com/locate/jpowsour

Short communication

Electrochemical property of $NH_4V_3O_8{\cdot}0.2H_2O$ flakes prepared by surfactant assisted hydrothermal method

Haiyan Wang[a], Kelong Huang[a,*], Suqin Liu[a], Chenghuan Huang[a], Wenjie Wang[a], Yu Ren[b]

[a] School of Chemistry and Chemical Engineering, Central South University, Changsha 410083, China
[b] EaStChem and School of Chemistry, University of St Andrews, St Andrews, Fife KY16 9ST, U.K.

ARTICLE INFO

Article history:
Received 27 February 2010
Received in revised form 27 June 2010
Accepted 8 July 2010
Available online 15 July 2010

Keywords:
Lithium ion battery
Ammonium trivanadate
Hydrothermal method
Electrochemical performance

ABSTRACT

$NH_4V_3O_8{\cdot}0.2H_2O$ is synthesized by sodium dodecyl sulfonate (SDS) assisted hydrothermal method and its electrochemical performance is investigated. The as-prepared material is characterized by X-ray diffraction (XRD), scanning electron microscopy (SEM), infrared (IR) spectrum, differential scanning calorimetry and thermal gravimetry (DSC/TG), cyclic voltammetry (CV), and charge–discharge cycling test. The results show a pure $NH_4V_3O_8{\cdot}0.2H_2O$ phase with flake-like morphology is obtained and the average flake thickness is about 150 nm. The $NH_4V_3O_8{\cdot}0.2H_2O$ electrode has a good lithium ion insertion/extraction ability with the highest discharge capacity of 225.9 mAh g^{-1} during 1.8–4.0 V versus Li at the constant current density of 15 mA g^{-1}. After 30 cycles, it still maintains a high discharge capacity of 209.4 mAh g^{-1}, demonstrating good cyclic stability. Interestingly, at the discharge process a new $(NH_4)Li_xV_3O_8{\cdot}0.2H_2O$ compound is formed due to the new lithium ion from lithium metal anode.

1. Introduction

During the past two decades, lithium ion battery has become dominant rechargeable battery in portable devices. It mainly involves the use of a layered structure transitional metal oxide, e.g. $LiCoO_2$ as positive electrode material. However, $LiCoO_2$ only enables to deliver a reversible capacity of about 140 mAh g^{-1} typically charged to 4.2 V ($x = 0.5$), which is much lower than its theoretical capacity (274 mAh g^{-1}). It is also difficult to meet the requirement of next generation rechargeable batteries for electrical vehicle [1–4]. Therefore, new positive electrode materials with higher discharge capacity have been proposed successively [5–9].

Layered compound of LiV_3O_8 is well-known as a promising cathode material for rechargeable lithium ion battery because of its low cost, high specific capacity, acceptable cyclability, and high rate capability [9–12]. Unfortunately, the electrochemical performance of this material is strongly affected by the preparation method and post-treatment condition [13]. LiV_3O_8 with low specific discharge capacity of 180 mAh g^{-1} was prepared by traditional solid state reaction of Li_2CO_3 and V_2O_5 reacted at 680 °C [9]. Liu et al. [12] obtained the LiV_3O_8 compound by a liquid phase method, delivering the discharge capacity of 274 mAh g^{-1}. Recently, single-crystalline LiV_3O_8 nanorods were fabricated [14], which exhibited 348 mAh g^{-1} in the first discharge at 20 mA g^{-1}.

Sometimes, NH_4VO_3, instead of V_2O_5, was used to prepare LiV_3O_8 [15]. In our previous work, in order to synthesize LiV_3O_8 phase with good electrochemical performance, NH_4VO_3 and LiOH were used as raw materials in the hydrothermal preparation. However, $NH_4V_3O_8$ with minor impurity of LiV_3O_8 was obtained at the end. To our surprise, such a mixed composite has acceptable electrochemical property, which means that $NH_4V_3O_8$ material may be of electrochemical performance. Recently, pure $NH_4V_3O_8$ and $NH_4V_3O_8{\cdot}xH_2O$ were prepared by several research groups [16–20]. Huang and Shan found that V_2O_5 could react with NH_3 under hydrothermal condition to produce the $NH_4V_3O_8$ [17]. $NH_4V_3O_8{\cdot}0.75H_2O$ nano-belt was prepared by hydrothermal approach and its electrical transport mechanism was investigated [18]. Furthermore, Torardi and Miao [20] prepared a new cathode material $(NH_4)_{0.9}V_3O_{7.9}F_{0.1}{\cdot}0.9H_2O$, which delivered the initial discharge capacity of 409 mAh g^{-1} at $C/80$ rate during 1.5–4.0 V versus Li but with very poor cyclic life. It is obvious that $NH_4V_3O_8$ and $NH_4V_3O_8{\cdot}xH_2O$ ($x \geq 0.75$) show different XRD patterns, indicating their crystal structures are different. For this reason, it is meaningful to study the electrochemical performance of $NH_4V_3O_8$ with a few amount of crystallographic H_2O or without crystallographic H_2O. Accordingly, pure $NH_4V_3O_8{\cdot}0.2H_2O$ material is prepared by a simple surfactant assisted hydrothermal approach with NH_4VO_3 as raw material. The electrochemical property of the as-prepared $NH_4V_3O_8{\cdot}0.2H_2O$ is reported in current work.

* Corresponding author. Tel.: +86 0731 88879850; fax: +86 0731 88879850.
E-mail address: klhuang@mail.csu.edu.cn (K. Huang).

0378-7753/$ – see front matter © 2010 Elsevier B.V. All rights reserved.
doi:10.1016/j.jpowsour.2010.07.022

2. Experimental

2.1. Synthesis and characterization

The starting material, NH_4VO_3 and the surfactant, sodium dodecyl sulfonate (SDS) were analytically pure. In a typical synthesis of $NH_4V_3O_8{\cdot}0.2H_2O$, 7.08 g NH_4VO_3 and 0.03 g SDS were dispersed in deionized water successively. In this work, surfactant SDS was used as soft template. Then proper amount of H_2SO_4 with the concentration of 1.5 mol L^{-1} was added into the solution to keep the pH of the solution at 2–3. The resultant dark wine-red solution was then transferred to 500 ml Teflon lined stainless steel autoclave. The total volume of the solution was about 350 ml. The autoclave was sealed and heated at 130 °C for 48 h. Before heating, 1.8 MPa N_2 was injected into the autoclave and subsequently about 3 MPa pressure was found after auto-generated pressure. After hydrothermal treatment, the obtained precipitate was filtered, washed with deionized water for three times. Finally, the precipitate was dried in a vacuum oven at 110 °C for 8 h and further annealed at 280 °C for 4 h in air.

For comparison, LiV_3O_8 was prepared by sol–gel method using citric acid as chelating agent, and NH_4VO_3, lithium acetate as raw materials. The molar ratio of Li:V:citric acid was 1.05:3:4.5. The citric acid solution was added drop-wise into the mixture solution of lithium acetate and NH_4VO_3 with the pH of 8–9. The reaction temperature was 50 °C. Then the mixture was treated at 80 °C to get the xero-gel. As follows the xero-gel was dried at 110 °C for 4 h in a vacuum oven and then it was ground to powder by hand. Finally, the precursor was calcined at 500 °C for 8 h and LiV_3O_8 was obtained.

The structure of obtained products was examined by X-ray diffractometer (Rigaku D/MAX2500) with a Cu Kα radiation. Infrared absorption spectrum was recorded using the AVATAR360 IR spectrometer. The surface morphology was observed by scanning electron microscopy (JSM6430F). DSC/TG experiments were carried out with a NETZSCH STA 449C differential scanning calorimeter at a ramping rate of 10 °C min^{-1}. And the temperature ranged from 50 to 800 °C. The batteries were disassembled in an Argon-filled glove box and some washed samples which were treated in DMC for 12 h and then baked 4 h at 100 °C in a vacuum oven were sealed in standard aluminum pan.

2.2. Electrochemical measurements

Electrochemical tests were operated using CR2016 coin-type cells, consisting of the cathode and a lithium metal anode, separated by a porous polyethylene film (Celgard 2500). The positive electrode contained 85% active material, 10% carbon black as conductive additive, and 5% polytetrafluoroethylene (PTFE) as binder. It was pressed onto a 100 mm^2 stainless steel mesh current collector at 15 MPa and then dried at 110 °C for 8 h in a vacuum oven in order to remove moisture. A commercial 1 M lithium-hexafluoro phosphate ($LiPF_6$) solution in a mixture of ethylene-carbonate (EC), dimethyl carbonate (DMC), diethyl carbonate (DEC) at a volume ratio of 1:1:1 was used as the electrolyte. The cells were cycled galvanostatically between 1.8 and 4.0 V versus Li at a desired current density with a Land tester system (CT2001A, Wuhan Land Electronic Co., Ltd.) at room temperature. Cyclic voltammetry (CV) test was carried out in electrochemical station (Shanghai Chenhua, China) at room temperature.

3. Results and discussion

Fig. 1 shows the X-ray diffraction pattern of the obtained powder. In comparison with a standard $NH_4V_3O_8$ (JCPDS card no. 88-1473), it is noted that the principal crystalline phase of the sample is pure $NH_4V_3O_8$ with the monocline structure (space group $p2_1/m$) [16,18]. Obviously, as observed, the crystal structure of current $NH_4V_3O_8$ is different from that of $NH_4V_3O_8{\cdot}0.75H_2O$ (JCPDS card no. 51-0376) [18,20]. The lattice parameters of this material could be indexed as follows: $a = 0.50043$ nm, $b = 0.84449$ nm, $c = 0.78755$ nm, which are closed to those of standard $NH_4V_3O_8$ (JCPDS card no. 88-1473 card, $a = 0.49994$ nm, $b = 0.84231$ nm, $c = 0.78491$ nm). Meantime, it was also found that the relative intensity of diffraction peak (0 0 1) is much higher than that reported in Ref. [19]. As we know, for LiV_3O_8, the higher the relative intensity of diffraction peak (0 0 1), the better the degree of crystallinity. Unfortunately, the preferential ordering of crystal is disadvantageous to the Li^+ intercalation and de-intercalation since it would lead to a long Li^+ diffusion path [21]. Thus, the high relative intensity of diffraction peak (0 0 1) of $NH_4V_3O_8$ will also affect the electrochemical performance of the material.

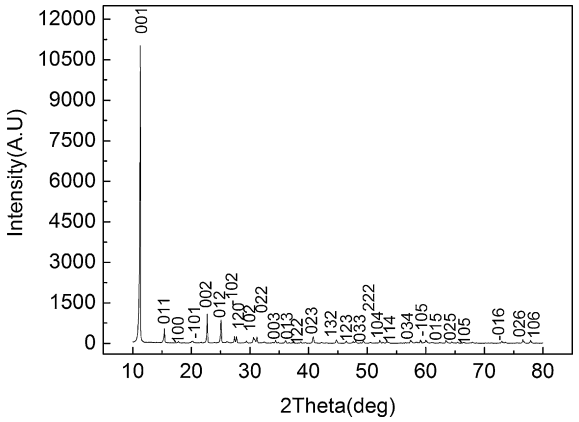

Fig. 1. X-ray diffraction pattern of the obtained powder by hydrothermal method.

The IR spectrum of the obtained $NH_4V_3O_8$ powder is shown in Fig. 2. As can be seen, there are several absorption bands at 3209.15, 1402.10, 1005.89, 967.32, 735.78, and 527.8 cm^{-1}, respectively. The bands at 1005.89 and 967.32 cm^{-1} are due to V=O stretching of distorted octahedral and distorted square pyramids, while those at 735.78 and 527.8 cm^{-1} are assigned to asymmetric and symmetric stretching vibration of V–O–V bonds [22]. At the same time, the bands at 3209.15 and 1402.1 cm^{-1} are attributed to the asymmetric stretching vibrations and the symmetric bending vibration of NH_4^+ [23]. Mai et al. considered [18] that they had prepared $NH_4V_3O_8$ by hydrothermal method; however, their obtained material actually consisted of $NH_4V_3O_8{\cdot}0.75H_2O$ since there were two obvious

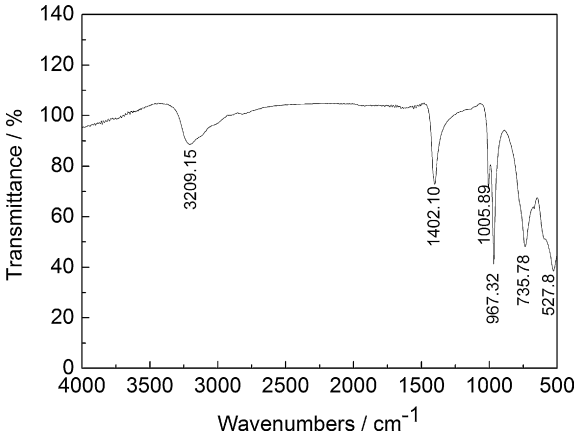

Fig. 2. Infrared spectrum of $NH_4V_3O_8{\cdot}0.2H_2O$.

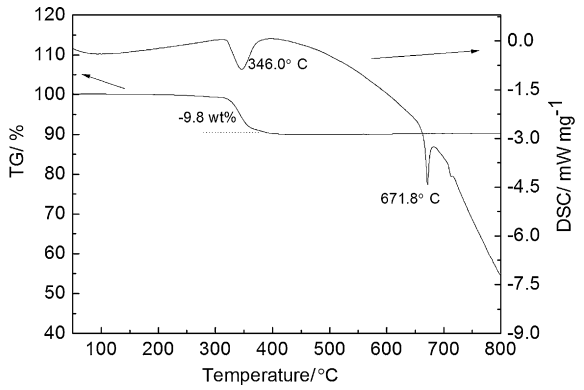

Fig. 3. DSC/TG curve of $NH_4V_3O_8{\cdot}0.2H_2O$.

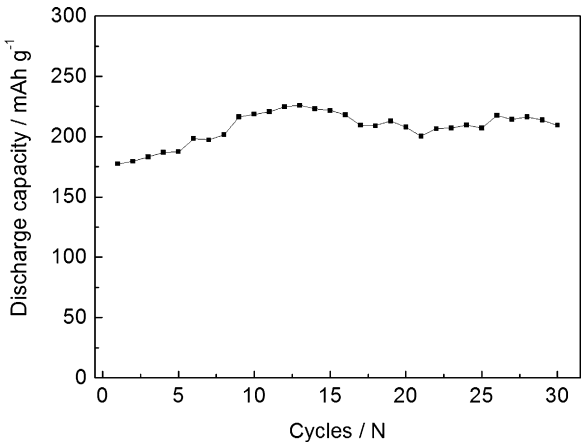

Fig. 5. Cyclic performance of $NH_4V_3O_8{\cdot}0.2H_2O$ electrode operated between 1.8 and 4.0 V versus Li at a current density of 15 mA g^{-1}.

bands at 3452 and 1614 cm^{-1} in the IR spectrum. In contrast, the $NH_4V_3O_8$ sample prepared in this work does not exhibit such evident characteristics. To make further certain, DSC/TG curve of prepared $NH_4V_3O_8$ powder is demonstrated in Fig. 3. Clearly, there is an exothermal peak at 346.0 °C, with a weight loss of about 9.8%, which should be attributed to the decomposition of $NH_4V_3O_8$ to V_2O_5, accompanied with the release of NH_3 and H_2O. Surprisingly, the weight loss of the as-prepared powder is little greater than that (8.7%) of $NH_4V_3O_8$ without crystallographic H_2O, illustrating that the as-prepared material contains a few amount of crystallographic H_2O (about 0.2 per unit). The results of XRD, IR and DSC/TG confirm that the as-prepared product is a pure $NH_4V_3O_8{\cdot}0.2H_2O$ phase, but the amount of crystallographic H_2O in $NH_4V_3O_8$ is less than those in previous reports [18,20]. As a matter of fact, the structure of $NH_4V_3O_8{\cdot}0.2H_2O$ is different from that of $NH_4V_3O_8{\cdot}0.75H_2O$ and $(NH_4)_{0.9}V_3O_{7.9}F_{0.1}{\cdot}0.9H_2O$ [18,20], implying that the amount of crystallographic H_2O in $NH_4V_3O_8$ would probably influence its structure, further its electrochemical performance.

Based on the above results, it could be concluded that $NH_4V_3O_8{\cdot}0.2H_2O$ could be successfully fabricated by a simple hydrothermal approach using NH_4VO_3 as raw material at lower reaction temperature (130 °C) than the literatures [17,18].

The morphology of the prepared $NH_4V_3O_8{\cdot}0.2H_2O$ is illustrated in Fig. 4. It has a flake-like shape and the average flake thickness is about 150 nm. Although, some of the flake-like powder are partially fused together to form larger particles, most of them appear to be separate. Particle morphology and particle size are very important factors to determine the electrochemical performance of electrode materials, e.g. LiV_3O_8 [12] since the intercalation and de-intercalation of Li^+ between the layers of LiV_3O_8 cathode is a diffusion process. Recently, surfactants have been widely used as soft template to prepare various kinds of nanostructure cathode materials. Undoubtedly, the SDS surfactant used in this work would play an important role in the formation of flake morphology.

Fig. 5 depicts the specific discharge capacity versus cyclic numbers at a current density of 15 mA g^{-1} during 1.8–4.0 V versus Li. It is demonstrated that the electrode is able to charge and discharge in the organic electrolyte, inferring that lithium ion can reversibly insert into and extract from $NH_4V_3O_8{\cdot}0.2H_2O$ crystal. The initial specific discharge capacity of this material is 177.3 mAh g^{-1} and enhances gradually to 225.9 mAh g^{-1}. After 30 cycles, the discharge capacity of 209.4 mAh g^{-1} is still maintained. Apparently, $NH_4V_3O_8{\cdot}0.2H_2O$ in this work has good cycling stability and shows better performance than LiV_3O_8 prepared by ordinary solid state reaction method [9]. It could be competitive with other lithium transition metal oxides ($LiCoO_2$, $LiMnO_2$, $LiNi_{1/3}Co_{1/3}Mn_{1/3}O_2$, etc.) [2,24–26]. The discharge curves of $NH_4V_3O_8{\cdot}0.2H_2O$ at different cycles are shown in Fig. 6. Apart from the first discharge curve, the other three discharge curves show exactly similar shape and three discharge voltage plateaus at 2.85, 2.41, and 1.95 V, respectively. In the case of the first discharge curve, the values of the three voltage plateaus are less than those of the subsequent cycle curves. It was reported that the sharp voltage drop from 4.0 to 3.0 V versus Li was attributed to the polarization process caused by the non-stable diffusion [12].

As mentioned above, the discharge capacity gradually increases for the first several cycles, which implies the $NH_4V_3O_8{\cdot}0.2H_2O$ should firstly undertake the obvious polarization, probably resulting from the presence of NH_4^+ group. The first two CV curves of $NH_4V_3O_8{\cdot}0.2H_2O$ and LiV_3O_8 electrode during 1.8–4.0 V versus Li

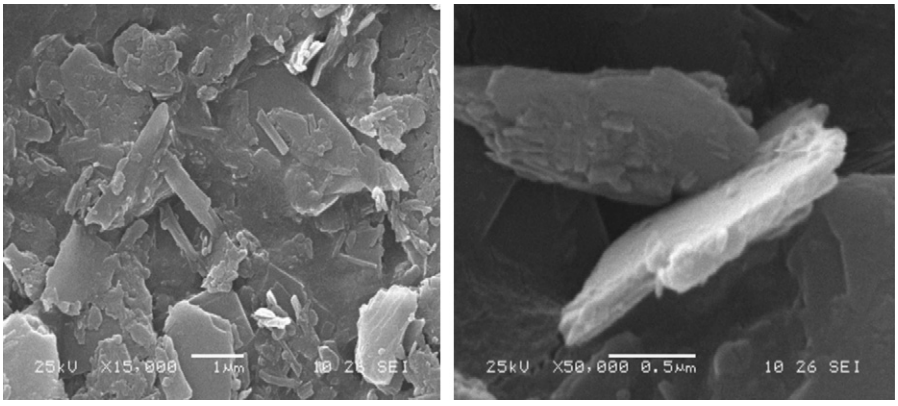

Fig. 4. SEM images of $NH_4V_3O_8{\cdot}0.2H_2O$ under different magnifications.

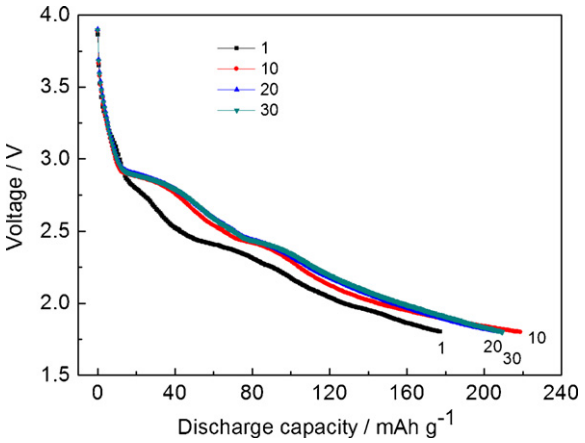

Fig. 6. Discharge curves of $NH_4V_3O_8{\cdot}0.2H_2O$ electrode at different cycles (1st, 10th, 20th, 30th) operated between 1.8 and 4.0 V versus Li at a current density of 15 mA g^{-1}.

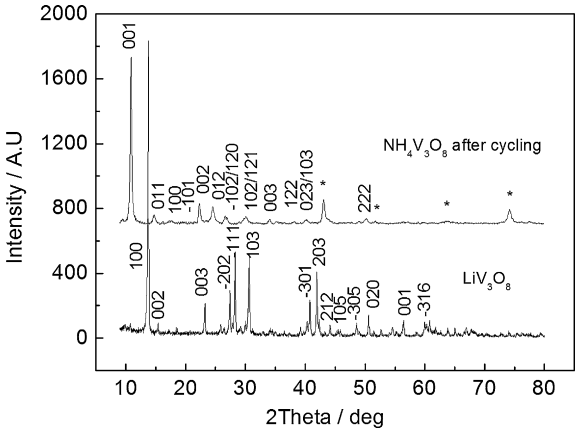

Fig. 8. XRD patterns of $NH_4V_3O_8{\cdot}0.2H_2O$ electrode with the cutting off voltage of 2.4 V versus Li after 15 cycles and as-prepared LiV_3O_8 powder by sol–gel method.

at a scanning rate of 0.1 mV s^{-1} are compared. As can be seen from Fig. 7(a), two obvious pairs of redox peaks, with the oxidation peaks at about 2.78 and 3.08 V and reduction peaks at about 2.27 and 2.75 V, respectively, are observed. Besides, there are also two weak reduction peaks, at about 3.14 and 3.35 V, respectively. However, their corresponding oxidation peaks seems not obvious. In the case of LiV_3O_8, it seems more complicate than that of $NH_4V_3O_8{\cdot}0.2H_2O$. At around 2.80 and 2.86 V, there are two overlapping oxidation peaks, and the corresponding reduction peaks show better separation. In addition, two weak redox peaks located at 3.35 and 3.50 V, respectively are also found. Appearance of redox peaks indicates steps reversible de-intercalation and intercalation of Li^+ in solid phase. In comparison with LiV_3O_8, clearly, $NH_4V_3O_8{\cdot}0.2H_2O$ electrode shows lower Li^+ de-intercalation voltages, which suggests the polarization of host increases when NH_4^+ group replaces Li^+ between $V_3O_8^-$ layers. More important, the intensity of the two main redox peaks in the second CV curve of $NH_4V_3O_8{\cdot}0.2H_2O$ electrode is larger than those in the first CV curve, which is in good accordance with the gradual increasing of discharge capacity (Fig. 5). In contrast, LiV_3O_8 electrode has no such phenomenon.

It should be pointed out that the high discharge capacity of $NH_4V_3O_8{\cdot}0.2H_2O$ must be due to the new lithium ion insertion from lithium metal anode during the discharge processes as there is little charge capacity in the first charge process. Actually, in $NH_4V_3O_8{\cdot}0.2H_2O$, V^{5+} cannot be oxidized any more. Hereby, it is sure that NH_4^+ group fails to extract from the host in the first charge. Does NH_4^+ group de-intercalate from the host, prior to Li^+ during the later cycles? The answer will be given in the following context.

The structure of $NH_4V_3O_8{\cdot}0.2H_2O$ electrode with the cutting off voltage of 2.4 V versus Li, after 15 cycles, was examined to judge whether the LiV_3O_8 phase appeared after Li^+ intercalation. Fig. 8 demonstrates the XRD patterns of $NH_4V_3O_8{\cdot}0.2H_2O$ electrode after cycling and LiV_3O_8 powder prepared in this work. With the exception of those diffraction peaks marked with *, which should be due to the stainless steel mesh, all the other lines in Fig. 8 are attributed to the diffraction peaks of $NH_4V_3O_8$. Clearly, in comparison with the XRD patterns of LiV_3O_8, no LiV_3O_8 phase is observed in $NH_4V_3O_8{\cdot}0.2H_2O$ electrode at the discharge process. It is important to note that the XRD pattern shifts toward low angle and the intensity of the main diffraction peaks decreases, compared with that of $NH_4V_3O_8{\cdot}0.2H_2O$ powder described in Fig. 1, resulting from the new Li^+ intercalation from lithium metal. Therefore, the compound, written as $(NH_4)Li_xV_3O_8{\cdot}0.2H_2O$ should be formed at discharge process.

Taking the highest discharge capacity of 225.9 mAh g^{-1} into consideration, the lithium ion inset quantity achieves 2.52, according to the calculated formula of specific capacity: $C = nF/3.6M$ (n is the quantity of lithium intercalated into $NH_4V_3O_8$, F is Faradic constant, 96485 $C\,mol^{-1}$, M is the molecular weight of $NH_4V_3O_8$). That is to say, the finally discharged electrode material after the 13th cycle becomes $(NH_4)Li_{2.52}V_3O_8{\cdot}0.2H_2O$.

Vanadium oxides and lithium vanadium oxide compounds possess good lithium ion extraction and insertion capability [9,27,28]. Among those materials, LiV_3O_8 is one kind of cathode materials with high capacity and acceptable structure stability (space group $p2_1/m$) [28]. Generally, the crystal LiV_3O_8 and $NH_4V_3O_8$ can be described as $V_3O_8^-$ puckered layers held together by lithium ions or NH_4^+ groups, respectively [17]. However, its ionic radius is about 147 pm, much larger than that of Li^+ (68 pm), Na^+ (95 pm). At the same time, different research groups reported the use of Na^+ doping cathode materials for lithium ion battery [29–31]. Usually, they

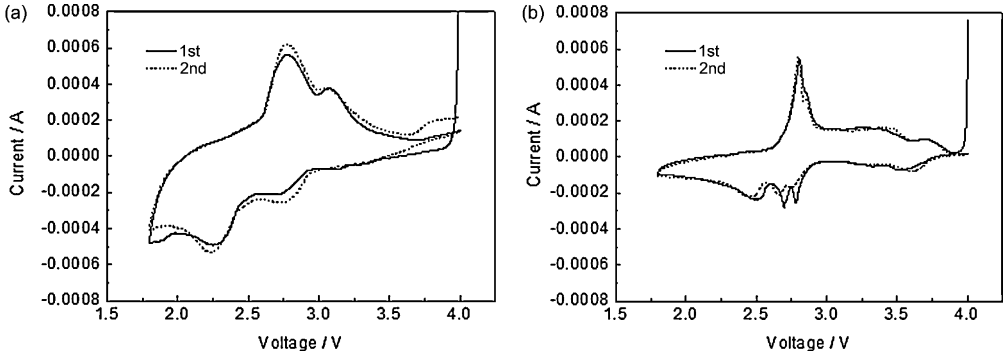

Fig. 7. The first two cyclic voltammetry curves of $NH_4V_3O_8{\cdot}0.2H_2O$ (a) and LiV_3O_8 electrode (b) between 1.8 and 4.0 V versus Li at a scanning rate of 0.1 mV s^{-1}.

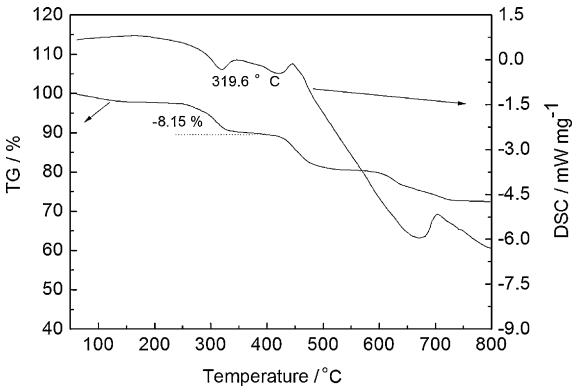

Fig. 9. DSC/TG curve of $(NH_4)Li_xV_3O_8$ electrode powder, with the cutting off voltage of 4.0 V versus Li after 3 cycles.

considered that Na^+ doped at Li^+ sites and proved that Na^+ could not extract easily from electrode material, but just acted as pillar to stable the crystal structure and enhanced the electronic conductivity. By density functional theory based on first-principles method, Ouyang et al. [30] found the diffusion energy barrier for Na ions along the one-dimensional diffusion pathway (*c*-direction) in the Na^+ doped $LiFePO_4$ was about 1.32 eV, while that for Li^+ was only about 0.415 eV. In the present work, NH_4^+ group, substituted the Li^+ site between $V_3O_8^-$ layers in LiV_3O_8, certainly, should increase the polarization of $NH_4V_3O_8$ crystal structure during Li^+ insertion and extraction because of its larger ionic radius and migration energy barriers than Li^+. It agrees well with the electrochemical results.

DSC/TG of $(NH_4)Li_xV_3O_8{\cdot}0.2H_2O$ electrode with the cutting off voltage of 4.0 V versus Li, after 3 cycles was carried out to estimate the residual amount of ammonium (Fig. 9). An exothermal peak at 319.6 °C is observed, with a weight loss of about 8.15%, which could be assigned to the decomposition of $(NH_4)Li_xV_3O_8{\cdot}0.2H_2O$. After removing the weight of carbon black and binder, the actual weight loss is about 9.6%, very closed to that of $NH_4V_3O_8{\cdot}0.2H_2O$ decomposition (9.8%). Based on the above results, we do not think that NH_4^+ group can extract from the $(NH_4)Li_xV_3O_8{\cdot}0.2H_2O$ during the later cycles. Therefore, NH_4^+ group in $NH_4V_3O_8{\cdot}0.2H_2O$ may just play the role of a structural stabilizer during cycling. Other molecules such as NH_3, CO_2 could also be intercalated between the LiV_3O_8 inter-layers, to improve the electrochemical performance of LiV_3O_8 [32].

4. Conclusions

In summary, a new battery cathode material, $NH_4V_3O_8{\cdot}0.2H_2O$ flake, is prepared by a simple, sodium dodecyl sulfonate assisted hydrothermal approach. XRD, IR, and DSC/TG results indicate that the obtained material is a pure $NH_4V_3O_8$ phase with about 0.2 mol crystallographic H_2O. It shows flake-like morphology with an average thickness of about 150 nm. The as-prepared $NH_4V_3O_8{\cdot}0.2H_2O$ electrode shows a good cycling stability which exhibits the greatest discharge capacity of 225.9 mAh g^{-1} and remains 209.4 mAh g^{-1} after 30 cycles.

Acknowledgements

Financial Support from the Major State Basic Research Development Program of China (973 Program) (No. 2010CB227204), the National Natural Science Foundation of China (No. 50972165), Graduate Degree Thesis Innovation Foundation of Central South University (1960-71131100017) is greatly appreciated.

References

[1] R. Yazami, N. Lebrun, M. Bonneau, M. Molteni, J. Power Sources 54 (1995) 389–392.
[2] S.Y. Lee, S.K. Kim, S. Ahn, Electrochem. Commun. 10 (2008) 113–117.
[3] H.L. Chen, C.P. Grey, Adv. Mater. 20 (2008) 2206–2210.
[4] M.S. Whittingham, Chem. Rev. 104 (2004) 4271–4301.
[5] Y.G. Liang, X.Y. Han, X.W. Zhou, J.T. Sun, Y.H. Zhou, Electrochem. Commun. 9 (2007) 965–970.
[6] S.B. Schougaard, J. Bréger, M. Jiang, C.P. Grey, J.B. Goodenough, Adv. Mater. 18 (2006) 905–909.
[7] H.S. Liu, Y. Yang, J.J. Zhang, J. Power Sources 162 (2006) 644–650.
[8] S.T. Myung, S. Komaba, N. Hirosaki, N. Kumagai, K. Arai, R. Kodama, Y. Terada, I. Nakai, J. Power Sources 119–121 (2003) 211–215.
[9] S. Panero, M. Pasquali, G. Pistoia, J. Electrochem. Soc. 130 (1983) 1225–1227.
[10] G. Pistoia, S. Panero, M. Tocci, R. Moshtev, V. Manev, Solid State Ionics 13 (1984) 311–318.
[11] J. Kawakita, T. Kato, Y. Katayama, T. Miura, T. Kishi, J. Power Sources 81–82 (1999) 448–453.
[12] G.Q. Liu, C.L. Zeng, K. Yang, Electrochim. Acta 47 (2002) 3239–3243.
[13] H.Y. Xu, H. Wang, Z.Q. Song, Y.W. Wang, H. Yan, M. Yoshimura, Electrochim. Acta 49 (2004) 349–353.
[14] H.M. Liu, Y.G. Wang, K.X. Wang, Y.R. Wang, H.S. Zhou, J. Power Sources 192 (2009) 668–673.
[15] H. Yang, J. Li, X.G. Zhang, Y.L. Jin, J. Mater. Process. Technol. 207 (2008) 265–270.
[16] B.Z. Lin, S.X. Liu, Acta Cryst. C55 (1999) 1961–1963.
[17] S.D. Huang, Y.K. Shan, Chem. Commun. (1998) 1069–1070.
[18] L.Q. Mai, C.S. Lao, B. Hu, J. Zhou, Y.Y. Qi, W. Chen, E.D. Gu, Z.L. Wang, J. Phys. Chem. B 110 (2006) 18138–18141.
[19] Q.Z. Yao, Chem. World 10 (2007) 585–588.
[20] C.C. Torardi, C.R. Miao, Chem. Mater. 14 (2002) 4430–4433.
[21] G. Pistoia, M. Pasquali, G. Wang, L. Li, J. Electrochem. Soc. 137 (1990) 2365–2370.
[22] B. Azambre, M.J. Hudson, O. Heintz, J. Mater. Chem. 13 (2003) 385–389.
[23] A. Dobley, K. Ngala, S.F. Yang, P.Y. Zavalij, M.S. Whittingham, Chem. Mater. 13 (2001) 4382–4386.
[24] K.S. Lee, S.T. Myung, J.S. Moon, Y.K. Sun, Electrochim. Acta 53 (2008) 6033–6037.
[25] Y. Makimura, T. Ohzuku, J. Power Sources 119–121 (2003) 156–169.
[26] S.H. Park, C.S. Yoon, S.G. Kang, H.S. Kim, S.I. Kim, S.I. Moon, Y.K. Sun, Electrochim. Acta 49 (2004) 557–563.
[27] G. Armstrong, J. Canales, A.R. Armstrong, P.G. Bruce, J. Power Sources 178 (2008) 723–728.
[28] M. Dubarry, J. Gaubicher, D. Guyomard, O. Durupthy, N. Steunou, J. Livage, N. Dupr, C.P. Grey, Chem. Mater. 17 (2005) 2276–2283.
[29] S.H. Park, S.S. Shin, Y.K. Sun, Mater. Chem. Phys. 95 (2006) 218–221.
[30] C.Y. Ouyang, D.Y. Wang, S.Q. Shi, Z.X. Wang, H. Li, X.J. Huang, L.Q. Chen, Chin. Phys. Lett. 23 (2006) 61–64.
[31] X.G. Yin, K.L. Huang, S.Q. Liu, H.Y. Wang, H. Wang, J. Power Sources 195 (2010) 4308–4312.
[32] V. Manev, A. Momchilov, A. Nassalevska, J. Power Sources 54 (1995) 501–507.